J|A|C|S
ARTICLES
Published on Web 06/20/2003

Solution NMR Characterization of the Electronic Structure and Magnetic Properties of High-Spin Ferrous Heme in Deoxy Myoglobin from *Aplysia limacina*

Dejian Ma,[†] Raffaella Musto,[‡] Kevin M. Smith,[†,§] and Gerd N. La Mar*[,†]

Contribution from the Department of Chemistry, University of California, Davis, California 95616, and the Department of Biochemical Sciences, University of Rome, "La Sapienza", Rome, Italy

Received March 20, 2003; E-mail: lamar@indigo.ucdavis.edu

Abstract: Solution ^{1}H NMR has been used to elucidate the magnetic properties and electronic structure of the prosthetic group in high-spin, ferrous deoxy myoglobin from the sea hare *Aplysia limacina*. A sufficient number of dipolar shifted residue signals were assigned to allow the robust determination of the orientation and anisotropy of the paramagnetic susceptibility tensor, χ. The resulting quantitative description of dipolar shifts allows a determination of the contact shifts for the heme. χ was found to be axial, with $\Delta\chi_{ax} = -2.07 \times 10^{-8}$ m^3/mol, with the major axis tilted ($\sim$76°) almost into the heme plane and in the general direction of the orientation of the axial HisF8 imidazole plane which coincides approximately with the β-,δ-meso axis. The factored contact shifts for the heme are shown to be consistent with the transfer of *positive* π spin density into one of the two components of the highest filled π molecular orbital, $3e_\pi$, and the transfer of *negative* π-spin density, via spin−spin correlation, into the orthogonal excited-state component of the $3e_\pi$ molecular orbital. The thermal population of the excited state leads to strong deviation from the Curie law for the heme substituents experiencing primarily the negative π-spin density. The much larger transfer of negative spin density via the spin-paired dπ orbital into the excited state $3e_\pi$ in high-spin iron(II) than in low-spin iron(III) hemoproteins is attributed to the much stronger correlation exerted by the four unpaired spin on the iron in the former, as compared to the single unpaired spins on iron in the latter.

Introduction

NMR spectra of paramagnetic hemoproteins are unique in that not only can they, under appropriate conditions, be interpreted almost as effectively as for a diamagnetic analogue to yield the molecular structure,[1−3] but the resulting hyperfine shifts near the active site yield a wealth of information on the electronic structure and magnetic properties of the active site not available for a diamagnetic derivative.[1,4,5] The majority of the systems studied possess low-spin, ferric hemin for which there exist relatively robust quantitative interpretive bases for both the contact and dipolar shifts.[5−16] While fewer high-spin ferric hemoproteins have been investigated in detail, the results provide a relatively simple, and for the contact shifts only empirical, correlation between molecular structure and electronic/magnetic properties.[5,17−24] The least understood iron oxidation/spin state is high-spin iron(II) heme, which is the only functional paramagnetic state of globins,[25,26] one of two functional states[27] of ferricytochromes *c*′, as well as one in many heme enzymes.[28,29]

There are two mechanisms that contribute to ^{1}H NMR hyperfine shifts, δ_{hf}. One is the contact shift for the ligands to the iron,[2] δ_{con}, given by

$$\delta_{con}{}^{i} = -Q\rho\langle S_z\rangle/\gamma_i B_o \qquad (1)$$

Q is a constant ($\sim$60−75 MHz for a methyl group experiencing

[†] University of California, Davis.
[‡] University of Rome.
[§] Present address: Department of Chemistry, Louisiana State University, Baton Rouge, LA 70803-1804.

(1) La Mar, G. N.; de Ropp, J. S. *Biol. Magn. Reson.* **1993**, *18*, 1−79.
(2) Bertini, I.; Luchinat, C. *Coord. Chem. Rev.* **1996**, *150*, 1−296.
(3) Banci, L.; Bertini, I.; Luchinat, C.; Turano, P. In *The Porphyrin Handbook*; Kadish, K. M., Smith, K. M., Guilard, R., Eds.; Academic Press: Boston, 1999; Vol. 5, pp 323−350.
(4) Bertini, I.; Turano, P.; Vila, A. J. *Chem. Rev.* **1993**, *93*, 2833−2933.
(5) La Mar, G. N.; Satterlee, J. D.; de Ropp, J. S. In *The Porphyrins Handbook*; Kadish, K. M., Smith, K. M., Guilard, R., Eds.; Academic Press: San Diego, 1999, Vol. 5, pp 185−298.
(6) Shulman, R. G.; Glarum, S. H.; Karplus, M. *J. Mol. Biol.* **1971**, *57*, 93−115.
(7) Traylor, T. G.; Berzinis, A. P. *J. Am. Chem. Soc.* **1980**, *102*, 2844−2846.
(8) Williams, G.; Moore, G. R.; Porteous, R.; Robinson, M. N.; Soffe, N.; Williams, R. J. P. *J. Mol. Biol.* **1985**, *183*, 409−428.
(9) Yamamoto, Y.; Nanai, N.; Chujo, R.; Suzuki, T. *FEBS Lett.* **1990**, *264*, 113−116.
(10) Emerson, S. D.; La Mar, G. N. *Biochemistry* **1990**, *29*, 1556−1566.
(11) Turner, D. L. *Eur. J. Biochem.* **1993**, *211*, 563−568.
(12) Brennan, L.; Turner, D. L. *Biochim. Biophys. Acta* **1997**, *1342*, 1−12.
(13) Banci, L.; Bertini, I.; Luchinat, C.; Pierattelli, R.; Shokhirev, N. V.; Walker, F. A. *J. Am. Chem. Soc.* **1998**, *120*, 8472−8479.
(14) Louro, R. O.; Correia, I. J.; Brennan, L.; Coutinho, I. B.; Xavier, A. V.; Turner, D. L. *J. Am. Chem. Soc.* **1998**, *120*, 13240−13247.
(15) Shokhirev, N. V.; Walker, F. A. *J. Biol. Inorg. Chem.* **1998**, *3*, 581−594.
(16) Turner, D. L. *J. Biol. Inorg. Chem.* **2000**, *5*, 328−332.
(17) Rajarathnam, K.; La Mar, G. N.; Chiu, M. L.; Sligar, S. G.; Singh, J. P.; Smith, K. M. *J. Am. Chem. Soc.* **1991**, *113*, 7886−7892.
(18) Banci, L.; Bertini, I.; Turano, P.; Vicens Oliver, M. *Eur. J. Biochem.* **1992**, *204*, 107−112.
(19) Bertini, I.; Gori, B.; Luchinat, C.; Vila, A. J. *Biochemistry* **1993**, *32* (2), 776−783.
(20) Clark, K.; Dugad, L. B.; Bartsch, R. G.; Cusanovich, M. A.; Lamar, G. N. *J. Am. Chem. Soc.* **1996**, *118*, 4654−4664.
(21) Caffrey, M.; Simorre, J.-P.; Brutscher, B.; Cusanovich, M.; Marion, D. *Biochemistry* **1995**, *34*, 5904−5912.
(22) Asokan, A.; de Ropp, J. S.; Newmyer, S. L.; Ortiz de Montellano, P. R. *J. Am. Chem. Soc.* **2001**, *123*, 4243−4254.
(23) Déméné, H.; Tsan, P.; Gans, P.; Marion, D. *J. Phys. Chem. B* **2000**, *104*, 2559−2569.

10.1021/ja035256u CCC: $25.00

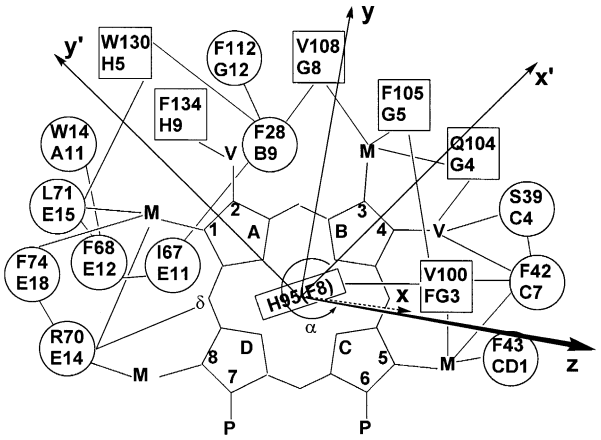

Figure 1. Schematic structure of the active site of *Aplysia limacina* Mb showing heme (and the Fisher numbering system), the axial His F8, and key assigned (completely or partially) residues on the proximal (rectangles) and distal (circles) sides of the heme. The lines between heme and residues and among residues reflect the observed (and expected) heme-residue and interresidue NOESY cross-peaks. The reference (x', y', z') and magnetic (x, y, z) coordinate systems are shown, where the angle β is the tilt of the major (z) magnetic axes from the heme normal (z'), α defines the projection of the tilt (and hence the direction) referenced to the x' axis, and the rhombic axes, x, y, when projected on the x', y' plane, are given by $\kappa \approx \alpha + \gamma$. The angle ϕ defines the relative orientation of the projection of the axial imidazole plane and the x' axis.

π spin density ρ_i, on an adjacent aromatic nucleus), and $\langle S_z \rangle$ is the spin magnetization that is approximately $\propto B_o/T$. The other is the dipolar shift, δ_{dip}, exerted by the iron on all nuclei, which is given[2,5,10,30] by

$$\delta_{dip} = (12\pi\mu_o N_a)^{-1}[3\Delta\chi_{ax}(3\cos^2\theta' - 1)R^{-3} + 2(\sin^2\theta'\cos^2\Omega')R^{-3}]\Gamma(\alpha,\beta,\gamma) \quad (2)$$

$\Delta\chi_{ax}$ and $\Delta\chi_{rh}$ are the axial and rhombic anisotropies of the paramagnetic susceptibility tensor, χ, in the magnetic coordinate system, x, y, z (or R, θ, Ω), where χ is diagonal. The angles θ', Ω' and distance R from the Fe define a proton in an arbitrary, iron-centered reference frame, z', y', z' (as provided by suitable crystal coordinates), and $\Gamma(\alpha,\beta,\gamma)$ is the standard Euler rotation that converts the reference (x', y', z' or R, θ', Ω') into the magnetic (x, y, z or R, θ, Ω) coordinate system (see Figure 1). Both the anisotropies of the tensor, χ, and its orientation ($\Gamma(\alpha,\beta,\gamma)$) can be determined by NMR if sufficient dipolar-shifted resonances can be assigned and crystal coordinates for their positions in the reference frame are available.[5,10,30]

Relatively few reports have addressed the heme hyperfine shifts in small, high-spin ferrous hemoproteins.[19,31−42] Only two systems have been studied in any detail (both anisotropy/orientation of χ and quantitated spin distribution for heme), deoxy Mb[43] from several mammals,[39,40] and one ferrocytochrome c'.[23,42] Heme methyl peaks have been assigned in two other ferrocytochromes c'[19,41] and an insect deoxy Mb,[44] but neither the anisotropies nor orientations of χ were determined. The two detailed studies[40,42] showed that the anisotropies arise overwhelmingly from zero-field splittings (as indicated by T^{-2} dependence of dipolar shifts) but that the tensors are strongly tilted away from the heme normal.[23,40,42] This is in sharp contrast to both low-spin [5] and high-spin iron(III) where the major magnetic axis is oriented close (within 15°) to the heme normal.[5,22−24] The directions of the tilts of the major magnetic axes in the two high-spin ferrous systems did not reveal what molecular structural properties of the active site (axial His imidazole plane orientation, nonligated distal water molecules) control the orientation.[23,40,42] Moreover, it has not been possible to propose a description of the nature of the spin transfer mechanism responsible for the heme contact shifts.[40,42] Finally, the magnitudes of the magnetic anisotropy differ significantly for the two systems[40,42] thought to possess very similar high-spin iron(II). Precedence for observing a major axis tilted strongly from the heme normal in high-spin ferrous hemoproteins exists in several other spectroscopic observables.[45,46]

One approach to improving the understanding of the NMR properties of high-spin ferrohemoprotein is to pursue quantitative studies of χ and heme spin distributions in homologous proteins which have been crystallographically characterized. In this context, the Mb from the sea hare *Aplysia limacina* provides an appropriate comparison to mammalian Mbs, since its axial His F8 imidazole plane is aligned close to the meso−Fe−meso vector,[47] while in mammalian Mb it is aligned closer to a N−Fe−N vector.[48] Whereas a crystal structure of *Aplysia* deoxy Mb has not been reported, structures have been reported for numerous other oxidation/spin/ligation states of *Aplysia* Mb[49−51] to indicate that the majority of residues maintain strongly

(24) Kao, Y.-H.; Lecomte, J. T. J. *J. Am. Chem. Soc.* **1993**, *115*, 9754−9762.
(25) Antonini, E.; Brunori, M. In *Hemoglobin and Myoglobin and Their Reactions with Ligands*; Elsevier: North-Holland Publishing: Amsterdam, 1971; pp 40−54.
(26) Ho, C.; Perussi, J. R. *Methods Enzymol.* **1994**, *232*, 97−138.
(27) Moore, G. R.; Pettigrew, G. W. In *Cytochromes c, Evolutionary, Structural and Physiochemical Aspects*; Rich, A., Ed.; Springer-Verlag: New York, 1990; pp 197−204.
(28) Ortiz de Montellano, P. R. *Acc. Chem. Res.* **1987**, *20*, 289−294.
(29) Ortiz de Montellano, P. R.; Wilks, A. *Adv. Inorg. Chem.* **2001**, *51*, 359−407.
(30) Williams, G.; Clayden, N. J.; Moore, G. R.; Williams, R. J. P. *J. Mol. Biol.* **1985**, *183*, 447−460.
(31) Wüthrich, K.; Hochmann, J.; Keller, R. M.; Wagner, G.; Brunori, M.; Giacometti, G. *J. Magn. Reson.* **1975**, *19*, 111−117.
(32) Emptage, M. H.; Xavier, A. V.; Wood, J. M.; Alsaadi, B. M.; Moore, G. R.; Pitt, R. C.; Williams, R. J. P.; Ambler, R. P.; Bartsch, R. G. *Biochemistry* **1981**, *20*, 58−64.
(33) La Mar, G. N.; Jackson, J. T.; Bartsch, R. G. *J. Am. Chem. Soc.* **1981**, *103*, 4405−4410.
(34) La Mar, G. N.; Jackson, J. T.; Dugad, L. B.; Cusanovich, M. A.; Bartsch, R. G. *J. Biol. Chem.* **1990**, *265*, 16173−16180.
(35) Yamamoto, Y.; Iwafune, K.; Chujo, R.; Inoue, Y.; Imai, K.; Suzuki, T. *J Biochem. Tokyo* **1992**, *112*, 414−420.
(36) Banci, L.; Bertini, I.; Turano, P.; Oliver, M. V. *Eur. J. Biochem.* **1992**, *204*, 107−112.
(37) Banci, L.; Bertini, I.; Marconi, S.; Pierattelli, R. *Eur. J. Biochem.* **1993**, *215*, 431−437.
(38) La Mar, G. N.; Dalichow, F.; Zhao, X.; Dou, Y.; Ikedo-Saito, M.; Chiu, M. L.; Sligar, S. G. *J. Biol. Chem.* **1994**, *288*, 29629−29635.
(39) Busse, S. C.; Jue, T. *Biochemistry* **1994**, *33*, 10934−10943.
(40) Bougault, C. M.; Dou, Y.; Ikeda-Saito, M.; Langry, K. C.; Smith, K. M.; La Mar, G. N. *J. Am. Chem. Soc.* **1998**, *120*, 2113−2123.
(41) Bertini, I.; Dikiy, A.; Luchinat, C.; Macinai, R.; Viezzoli, M. S. *Inorg. Chem.* **1998**, *37*, 4814−4821.
(42) Tsan, P.; Caffrey, M.; Daku, M. L.; Cusanovich, M.; Marion, D.; Gans, P. *J. Am. Chem. Soc.* **1999**, *121*, 1795−1805.
(43) Abbreviations used: Mb, myoglobin; Hb, hemoglobin; NOE, nuclear Overhauser effect; NOESY, two-dimensional nuclear Overhauser spectroscopy; TOCSY, two-dimensional total correlation spectroscopy; DSS, 2,2-dimethyl-2-silapentane-5-sulfonate; MO, molecular orbital.
(44) La Mar, G. N.; Anderson, R. R.; Budd, D. L.; Smith, K. M.; Langry, K. C.; Gersonde, K.; Sick, H. *Biochemistry* **1981**, *20*, 4429−4436.
(45) Kent, T. A.; Spartalian, K.; Lang, G. *J. Chem. Phys.* **1979**, *71*, 4899−4908.
(46) Winkler, H.; Ding, X.-Q.; Burkardt, M.; Trautwein, A.; Parak, F. *Hyperfine Interact.* **1994**, *71*, 875−878.
(47) Bolognesi, M.; Onesti, S.; Gatti, G.; Coda, A.; Ascenzi, P.; Giacometti, A.; Brunori, M. *J. Mol. Biol.* **1989**, *205*, 529−544.
(48) Kuriyan, J.; Wilz, S.; Karplus, M.; Petsko, G. A. *J. Mol. Biol.* **1986**, *192*, 133−154.
(49) Bolognesi, M.; Coda, A.; Frigero, F.; Gatti, G.; Ascenzi, P.; Brunori, M. *J. Mol. Biol.* **1989**, *205*, 529−544.
(50) Mattevi, A.; Gaffi, G.; Coda, A.; Rizzi, M.; Ascenzi, P.; Brunori, M.; Bolognesi, M. *J. Mol. Recognit.* **1991**, *4*, 1−6.
(51) Conti, C.; Moser, C.; Rizzi, M.; Mattevi, A.; Lionetti, C.; Coda, A.; Ascenzi, P.; Brunori, M.; Bolognesi, M. *J. Mol. Biol.* **1993**, *233*, 498−508.

conserved positions relative to the iron in different oxidation/ligation/spin states. We report herein a detailed ^{1}H NMR assignment of both the heme and dipolar-shifted protons in *Aplysia* deoxy Mb that allows us to determine the orientation and anisotropy of χ as well as quantitate the unpaired spin density distribution on the heme.

Experimental Section

Protein Samples. Recombinant *Aplysia limacina* Mb was expressed in *E. coli* and purified as described in detail previously.[52] The deoxy Mb complex was formed by adding 3 equiv of dithionite to thoroughly degassed 2.0 mM ^1H_2O and ^2H_2O metMb samples at pH ~8.2. The prepared deoxy Mb samples reproduced both the previously reported optical [52] and ^{1}H NMR spectra.[31] The *Aplysia* Mb samples reconstituted with specifically deuterium-labeled hemins were generated by preparation of apo-Mb using standard methods.[53] The desired heme was titrated to yield 1:1 apo-Mb:heme stoichiometry, as determined spectrophotometrically, and as reported in detail for the same complexes previously.[54] The four labeled hemins are 1-C^{2}H$_3$,3-C^{2}H$_3$-hemin, 5-C^{2}H$_3$-hemin, 1-C^{2}H$_3$,8-C^{2}H$_3$-hemin, and 2-C$_\alpha$^{2}H1-C$_\beta$^{2}H$_2$-hemin and led to ~0.5 mM ^2H_2O solutions of deoxy Mb and those described previously.[54]

NMR Spectra. ^{1}H NMR spectra were recorded at 500 MHz on a Bruker AVANCE spectrometer. Nonselective T_1s were estimated from the null in the inversion recovery after a 180° pulse, ($T_1 \approx \tau_{null}/\ln 2$). Chemical shifts were referenced to 2,2-dimethyl-2-silapentane-5-sulfonate, DSS, via the residual solvent signal. Uncertainties are estimated at ±15% for resolved peaks and ±25% for partially resolved peaks. The R^{-6}_{Fe-i} dependence of nonselective T_1s[1,55] together with a $T_1 \approx 50$ ms for a heme methyl ($R_{Fe} \approx 6.1$ Å), a measured T_{1i} (in ms) for proton i is related to its distance to the iron, R_{Fe-i} via

$$R_{Fe-i} = 3.1T_{1i}^{1/6} \quad (3)$$

Reference spectra were recorded at 1 to 3 s^{-1} repetition rates over a 16 kHz spectral width and at 5 s^{-1} on a 50.0 kHz spectral width with presaturation of the residual solvent signal. WEFT spectra[56] were collected at a repetition rate of 5 s^{-1} and with relaxation delays between 260 and 100 ms. Steady-state NOE difference spectra were obtained by saturating 30−60% the desired resonance for 100 ms and subtracting the trace from a trace recorded when the same saturation power was applied well off-resonance to all peaks, as discussed in detail previously.[1,57] NOESY[58] (bandwidth 60 kHz, τ_m = 40 ms) and clean-TOCSY[59] (40 kHz, τ_m = 20 ms) ^{1}H NMR spectra in ^2H_2O were recorded over the temperature range 30° to 45 °C at 500 MHz at a repetition rate of 3 s^{-1} (to enhance cross-peaks for relaxed, at the expense of relatively weakly relaxed, protons) using 512 t1 blocks of 2048 t2 points, each consisting of 192 scans per block. The 2D data were processed with a 30°-shifted sine-squared function and zero-filled to 2048 × 2048 points prior to Fourier transformation.

Magnetic Axes Determination. The magnetic axes were determined by a least-squares search for the minimum in the error function:[10,30]

$$F/n = \sum_{i=1}^{n} |\delta_{dip}(obs) - \delta_{dip}(calc)|^2 \quad (4)$$

where the calculated dipolar shift in the reference coordinate system, x', y', z' or R, θ' Ω', (crystal coordinates[47]) is given by eq 2, with $\Delta\chi_{ax}$ and $\Delta\chi_{rh}$ as the axial and rhombic anisotropies of the diagonal paramagnetic susceptibility tensor. The observed dipolar shift, δ_{dip}(obs), is given by

$$\delta_{dip}(obs) = \delta_{DSS}(obs) - \delta_{DSS}(dia) \quad (5)$$

where δ_{DSS}(obs) and δ_{DSS}(dia) are the chemical shifts, in ppm, referenced to DSS, for the paramagnetic Mb complex and an isostructural diamagnetic complex, respectively. In the absence of an experimental δ_{DSS}(dia), it may be reliably estimated from the available molecular structure of *Aplysia* metMb[47] via

$$\delta_{DSS}(dia) = \delta_{tetr} + \delta_{sec} + \delta_{rc} \quad (6)$$

where δ_{tetr}, δ_{sec}, and δ_{rc} are the chemical shifts of an unfolded tetrapeptide relative to DSS,[60] the effect of secondary structure[61] and ring currents[62] on the shift, respectively. The contact shift for the heme and axial His F8 is determined by

$$\delta_{con} = \delta_{hf} - \delta_{dip}(calc) = \delta_{DSS}(obs) - \delta_{DSS}(dia) - \delta_{dip}(calc) \quad (7)$$

Results

Assignment Protocols. The assignments rely on three experimental parameters, scalar (TOCSY)[59] connections within a residue, dipolar ($\propto r_{ij}^{-6}$), (NOE[63] or NOESY[58]) connections, and paramagnetic relaxation;[55] eq 3 ($\propto R_{Fe-i}^{-6}$).

The resolved portions of the 500 MHz ^{1}H NMR spectra of *Aplysia* deoxy Mb in ^2H_2O at several temperatures are illustrated in Figure 2A−C. Peaks are labeled by upper case letters for the major (~75%) and lower case letters for the minor (~25%) of the heme orientational isomers,[54,64,65] using the Fisher notation for the heme. The spectrum at 30 °C in Figure 2 reveals six resolved or partially resolved methyl group signals (three-proton signals over a wide temperature range), one low-field, five high-field, all with T_1s ≈ 50 ± 10 ms (Tables 1, 2). Hence, relaxation properties are insufficient to clearly discriminate between heme and amino acid methyl peaks. Moreover, because of the relatively small hyperfine shift dispersion, the spectral congestion due to heme orientational disorder[54,64,65] (note resolved minor component peaks labeled 3-cH$_3$, 1-ch$_3$ and 5-ch$_3$ in Figure 2A), moderate T_1 relaxation and significant Curie (T_2) relaxation,[66,67] it was not possible to detect the key TOCSY cross-peak for several of the strongly hyperfine shifted peaks. In these cases, assignments were guided by the expected relaxation (eq 3) and dipolar (NOESY, NOE) contacts among heme substituents and between heme and nearby residues, as predicted in the metMb crystal structure.[47] Difficulties with resolution are partially solved by carrying out the NOESY and relaxation

(52) Cutruzzola, F.; Allocatelli, C. T.; Brancaccio, A.; Brunori, M. *Biochem. J.* **1996**, *314*, 83−90.
(53) Teale, F. W. J. *Biochim. Biophys. Acta* **1959**, *35*, 543.
(54) Pande, U.; La Mar, G. N.; Lecomte, J. T. J.; Ascoli, F.; Brunori, M.; Smith, K. M.; Pandey, R. K.; Parish, D. W.; Thanabal, V. *Biochemistry* **1986**, *25*, 5638−5646.
(55) Banci, L.; Bertini, I.; Luchinat, C. *Nuclear and electronic relaxation*; VCH: Weinheim, 1991.
(56) Gupta, R. K. *J. Magn. Reson.* **1976**, *24*, 461−465.
(57) Thanabal, V.; de Ropp, J. S.; La Mar, G. N. *J. Am. Chem. Soc.* **1987**, *109*, 7516−7525.
(58) Jeener, J.; Meier, B. H.; Bachmann, P.; Ernst, R. R. *J. Chem. Phys.* **1979**, *71*, 4546−4553.
(59) Griesinger, C.; Otting, G.; Wüthrich, K.; Ernst, R. R. *J. Am. Chem. Soc.* **1988**, *110*, 7870−7872.
(60) Bundi, A.; Wüthrich, K. *Biopolymers* **1979**, *18*, 285−297.
(61) Wishart, D. S.; Sykes, B. D.; Richards, F. M. *J. Mol. Biol.* **1991**, *222*, 311−333.
(62) Cross, K. J.; Wright, P. E. *J. Magn. Reson.* **1985**, *64*, 220−231.
(63) Neuhaus, D.; Williamson, M. *The Nuclear Overhauser Effect*; VCH Publishers: New York, 1989.
(64) Peyton, D. H.; La Mar, G. N.; Pande, U.; Ascoli, F.; Smith, K. M.; Pandey, R. K.; Parish, D. W.; Bolognesi, M.; Brunori, M. *Biochemistry* **1989**, *28*, 4880−4887.
(65) Nguyen, B. D.; Xia, Z.; Cutruzzolá, F.; Travaglini Allocatelli, C.; Brancaccio, A.; Brunori, M.; La Mar, G. N. *J. Biol. Chem.* **2000**, *275*, 742−751.
(66) Gueron, M. *J. Magn. Reson.* **1975**, *19*, 58−66.
(67) Johnson, M. E.; Fung, L. W.-M.; Ho, C. *J. Am. Chem. Soc.* **1977**, *99*, 1245−1250.

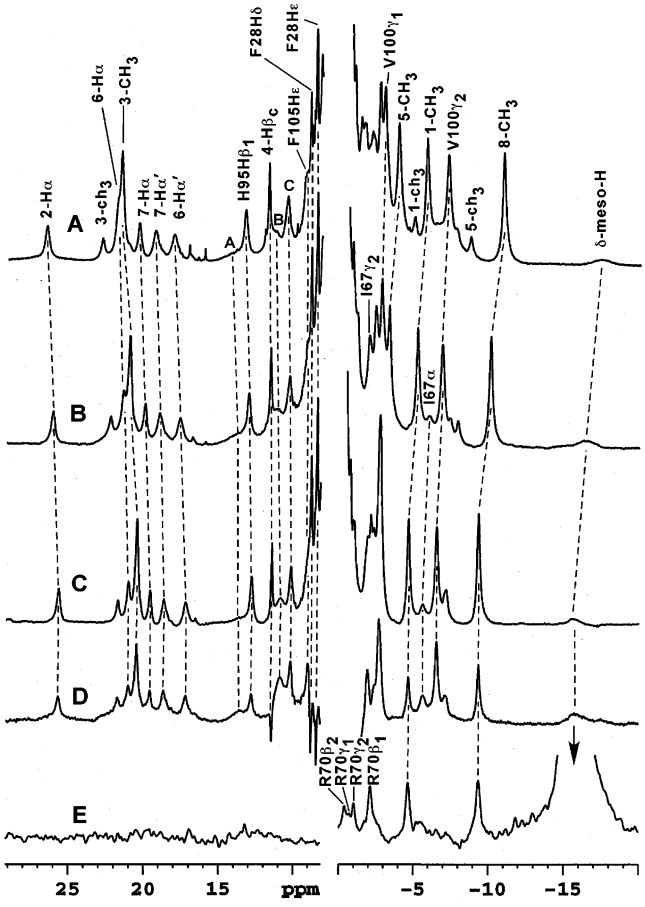

Figure 2. Resolved portions of the 500 MHz ^{1}H NMR spectra of *Aplysia* deoxy Mb in ^2H_2O, pH 8.5 at (A) 30 °C, (B) 36.2 °C, and (C) 41.2 °C, illustrating the strong and differentiated temperature dependence of both position and line width of resolved resonances; (D) Partially relaxed spectrum at 41.2 °C (repetition rate 3 s^{-1}, relaxation delay 70 ms), illustrating the position and relaxation properties of strongly relaxed lines not readily recognized in the normal NMR trace; and (E) steady-state NOE difference spectra upon saturating the strongly relaxed (δ-meso-H) peak at −15 ppm. Resonances for the major (i.e., 5-CH_3), minor (i.e., 5-ch_3) are labeled by upper case and lower case letters, respectively.

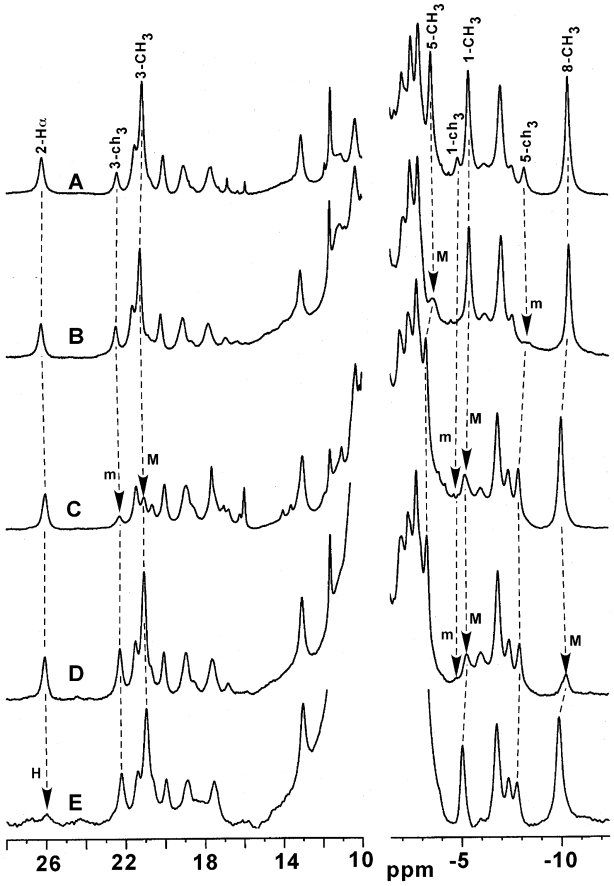

Figure 3. Resolved portions of the ^{1}H NMR spectra of *Aplysia* deoxy Mb in ^2H_2O, pH 8.6 at 35 °C containing (A) native hemin; (B) 5-C^2H_3-hemin; (C) 1-C^2H_3,3-C^2H_3-hemin; (D) 1-C^2H_3,8-C^2H_3-hemin; and (E) 2-Cα^2H-C$_\beta{}^2H_2$-hemin. M and m designate methyls in major and minor heme orientational isomers in solution, respectively. The selective loss of intensity is shown by vertical arrows and allows the unambiguous assignment of all four heme methyls for the major (∼80%) deoxy Mb component (heme orientation as drawn in Figure 1) and three of the four heme methyls (positions 1, 5, 3) for the minor (∼20%) deoxy Mb component (heme rotated by 180° about α,γ-meso axis relative to that in Figure 1).

measurements over a wide temperature range.[68] Last, as initial assignments of residues establish that δ_{dip} exhibits strictly T^{-2} dependence,[40,42] predicted intercepts in a plot of shift versus T^{-2} can be used to infer the functionality of proton sets. The key role of heme-residue contacts in the assignment protocol demands that the heme substituents be assigned first and unambiguously, which, in the absence of an isotope-labeled polypeptide, dictates the use of isotope-labeled hemes.[40]

Isotope Labeling. The resolved portions of the 500 MHz ^{1}H NMR spectra of *Aplysia* deoxy Mb at 35 °C containing native hemin and four different isotope-labeled hemins are illustrated in Figure 3A−E. The selective loss of intensity (vertical arrows) of major component (Mi) and minor component (m_i) methyl groups uniquely assigns (Figure 3A−D) the four heme methyls of the major, and all but the 8-CH_3 (which is not resolved) of the minor component. Deuteration of the 2-vinyl group leads to loss of only a single low-field proton peak (Figure 3E) which, in combination with its T_1 ∼50 ms (Table 1), identifies the $2H_\alpha$ and dictates that neither $2H_{\beta c}$ nor $2H_{\beta e}$ are resolved. These assignments are listed in Table 1.

Steady-State NOEs. The ^{1}H NMR spectrum of *Aplysia* deoxy Mb in ^1H_2O, as those of all other investigated monomeric deoxy globins,[5,26,38,69] exhibits one strongly relaxed ($T_1 \approx 10$ ms), labile proton peak near 90 ppm (not shown) that can only arise from the His F8 ring $N_\delta H$.[5,69] Saturation of this peak (not shown) exhibits a weak NOE to a moderately relaxed, resolved, low-field shifted single proton peak at ∼13 ppm at 30° (Figure 2A) that is uniquely identified as the His95(F8) $C_{\beta 1}H$ via its T_1. A strong NOE (not shown), as well as a strong NOESY cross-peak to $C_{\beta 1}H$ (Figure 4G), locates the geminal partner His95-(F8) $C_{\beta 2}H$. Last, the saturation of the broad and strongly relaxed ($T_1 \approx 10$ ms, $R_{Fe} \approx 4.5$ Å via eq 7), extreme high-field peak (Figure 2E) leads to comparable NOEs to both 1-CH_3 and 8-CH_3, uniquely assigning the δ-meso-H. The reference spectrum at 41.2 °C in Figure 2C suggests the presence of some strongly relaxed, $T_1 \lesssim 10$ ms, peaks labeled A,B under narrower peaks in the 10−18 ppm window. A WEFT trace[56] that suppresses weakly relaxed protons shows these peaks more clearly, with T_1 estimates 5 and 10 ms, respectively (Figure 2D),

(68) Qin, J.; La Mar, G. N. *J. Biomol. NMR* **1992**, *2*, 597−618.

(69) La Mar, G. N. In *Biological Applications of Magnetic Resonance*; Shulman, R. G., Ed.; Academica Press: New York, 1979; pp 305−343.

Table 1. ^{1}H NMR Spectral Parameters for the Heme and Axial His in *Aplysia Limacina* Deoxy Mb

residue	proton	δ_{DSS}(obs)[a]	T_1, ms[b]	δ_{DSS}(dia)[c]	δ_{hf}[d]	case II δ_{dip}(calc)[e]	case II δ_{con}(calc)[f]	*cytochrome c′*[g]	sperm whale deoxy Mb[h]
heme	1-CH_3	−5.20	60	3.6	−8.8	−5.7	−3.1	−1.8	7.2
	3-CH_3	20.98	60	3.8	17.2	2.7	15.0	15.5	5.0
	5-CH_3	−3.32	60	2.5	−5.9	−5.2	−0.7	−5.8	15.7
	8-CH_3	−10.09	60	2.6	−13.7	−4.8	−8.9	−9.7	3.5
	2Hα	26.10	45	8.4	17.7	0.8	16.9		
	2Hβc	−0.11		5.7	−5.8	0.8	−6.6		
	4Hα	−0.89		8.6	−9.5	−6.6	−2.9		
	4Hβc	11.56	∼80	6.3	5.3	−1.9	7.2		
	4Hβt	8.09		6.6	1.5	−1.8			
	6Hα	21.43	60	4.2	17.2	−0.5	17.7	18	7.9
	6Hα′	17.61	45	4.2	13.4	1.4	12.0	13	1.7
	7Hα	19.95	60	4.2	15.7	4.1	11.6	20	6.9
	7Hα′	18.99	45	4.2	14.8	1.3	13.6	41	11
	α-meso-H	i		9.9		9.6			
	β-meso-H	i		9.3		−17.9			
	γ-meso-H	i		10.0		9.6			
	δ-meso-H	−16.4	∼10	9.9	−26.3	−19.0	−7.3		
His95(F8)	Cβ1H	13.62	65	1.2	11.8	0.0	11.8		
	Cβ2H	5.97		0.8	5.1	2.3	2.8		

[a] Chemical shift, in ppm, referenced to DSS, in ^2H_2O solution at pH 8.5 and 36 °C. [b] T_1, in ms, estimated by null point in a 180°−τ−90° T_1 determination. [c] Chemical shift for diamagnetic analogue given by eq 6. [d] Hyperfine shifts given by eqs 6 and 7. [e] Dipolar shift obtained by eq 2 with $\Delta\chi_{ax} = -2.07 \times 10^{-9}$ m^3/mol, $\alpha = 310°$, $\beta = 76°$ (case II magnetic axes). [f] Contact shift obtained via eqs 2, 5, and 7 using case II magnetic axes. [g] Published data[42] for *R. capsulatus* ferrocytochrome *c′*. [h] Published data[40] for sperm whale deoxy Mb. [i] Not assigned.

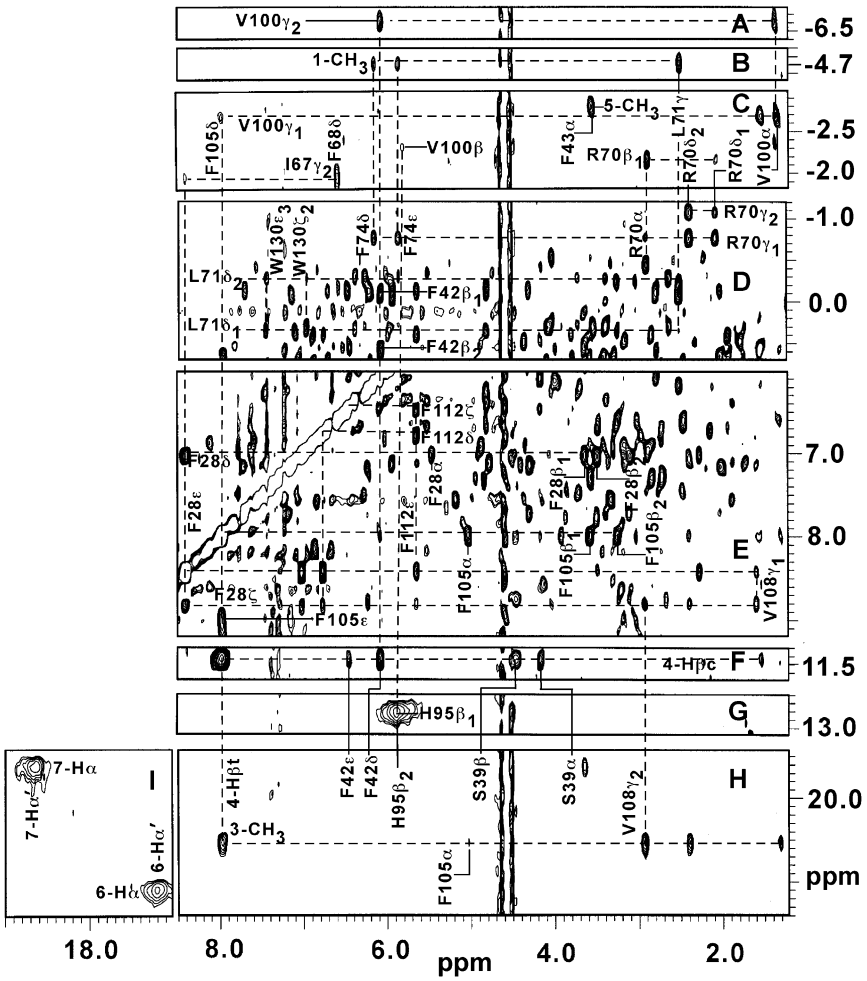

Figure 4. Low-field portion of the 500 MHz ^{1}H NMR NOESY spectrum (repetition rate 3 s^{-1}, mixing time 50 ms) of *Aplysia* deoxy Mb in ^2H_2O 100 mM phosphate, pH 8.5 at 36° illustrating key interresidue (A, C−E), intraresidue (G), heme-residue (B, C, F, H), and intraheme (F, H, I) dipolar connections.

and also locates an additional relaxed signal at 10 ppm with T_1 ≈ 20 ms (labeled $H_{105\epsilon}$). The resonances labeled A−C are too strongly relaxed and too close to the diamagnetic envelope to allow detection of steady-state NOEs that can be separated from off-resonance effects and artifacts, and hence, no information for assignments is available except the T_1s; peak B may have

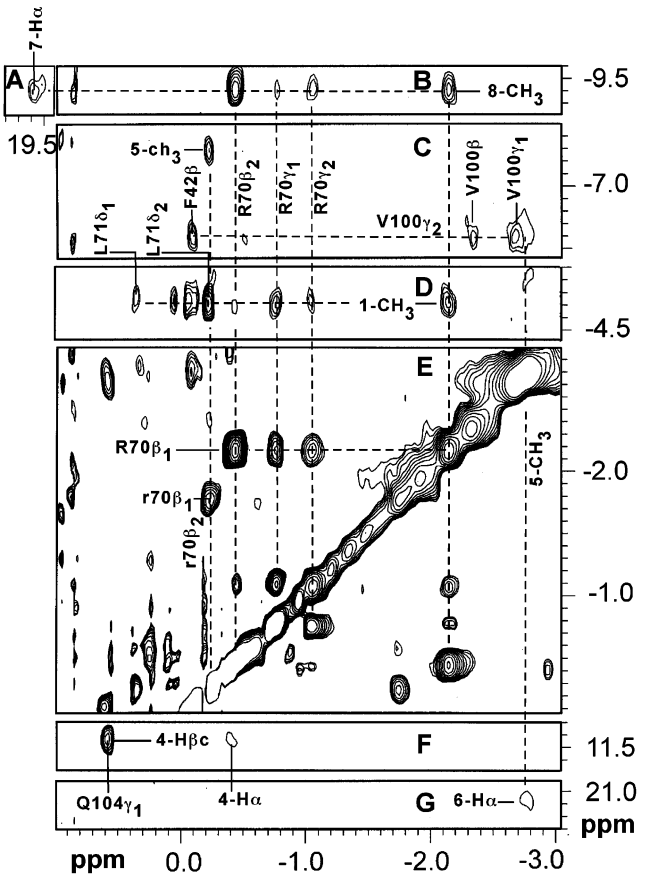

Figure 5. High-field portion of the 500 MHz ^{1}H NMR NOESY spectrum (repetition rate 3 s^{-1}, mixing time = 50 ms) illustrating key intraheme (A, F, Q), heme-residue (B, D, F, G), intraresidue (C, E), and interresidue (C) dipolar contacts.

an intensity larger than one proton; all three peaks exhibit only weak temperature dependence.

Heme Assignments. NOESY spectra that allow the assignment of the remainder of the heme are shown in Figures 4 and 5. Two pairs of low-field protons, labeled $H_{6\alpha}$, $H'_{6\alpha}$ and $H_{7\alpha}$, $H'_{7\alpha}$ (Figure 2A), exhibit very strong NOESY cross-peaks within each pair (Figure 4I), with $H_{6\alpha}$ and $H_{7\alpha}$ exhibiting NOESY cross-peaks to the assigned 5-CH_3 (Figure 5G) and 8-CH_3 (Figure 5A), respectively. The large hyperfine shifts, geminal nature of each pair, and proximity to the pyrrole C or D methyls, together with their relaxation ($T_1 \approx 50-70$ ms) indicative of protons α to the heme, identify the propionate $6H_\alpha$s and $7H_\alpha$s. The relaxation of $H4_{\beta c}$ ($T_1 \approx 80$ ms), and the geminal partner $4H_{\beta c}$ (Figure 4F), and the NOESY to 3-CH_3 (Figure 4H) identify the 4-vinyl H_βs; a NOESY cross-peak to an unresolved but broad and relaxed proton at -0.2 ppm locates the $H_{4\alpha}$ (not shown). The unambiguously assigned 2-vinyl $H_{2\alpha}$ exhibits NOESY cross-peaks near $\sim$0 ppm which represent at least $H_{2\beta c}$, and possibly also $2H_{\beta t}$ (not shown). Candidates for the propionate H_βs are observed upon saturating the $6H_\alpha$ and $7H_\alpha$s (not shown), but since these protons do not play any role in subsequent assignments, they are hence ignored. The heme assignments are listed in Table 1.

Active Site Residue Assignments. TOCSY connections (not shown; see Supporting Information) among a series of upfield shifted protons with significant dipolar shift (three of which are at least partially resolved single proton peaks at one temperature) yield a complete seven-spin system with four of the protons exhibiting NOESY cross-peaks to 1-CH_3 (Figure 5B) and 8-CH_3 (Figure 5D). The pattern of NOESY cross-peaks to the two heme methyls, together with expected steady-state NOEs from the δ-meso-H (Figure 2E), unambiguously and stereospecifically identifies the complete Arg70(E14).[47] Two weakly dipolar shifted, aliphatic three-spin systems are detected (Supporting Information), one of which exhibits NOESY cross-peaks to the 1-CH_3 (Figure 5C). The variable temperature intercepts (Table 2) indicate that the two upfield peaks are due to methyls. The NOESY cross-peak to the 1-CH_3 of this isopropyl fragment identifies the terminus of Leu71(E15). An AMX spin system whose temperature dependence reflects a $C_\alpha H$ for one proton (Table 2) locates a $C_\alpha HC_\beta H_2$ fragment whose NOESY cross-peaks to the 5-CH_3 (Figure 5C) and 4-vinyl (not shown) are consistent with arising from the backbone of Phe42-(C7). This assignment is confirmed by NOESY cross-peaks of this fragment to a TOCSY-detected (not shown; see Supporting Information), three-spin aromatic ring (Figure 4D) which also exhibits the NOEs to 4-H_β (Figure 4F) as predicted solely for Phe42(C7). A three-spin (not shown) aliphatic fragment exhibits NOESY cross-peaks to both the Phe42(C7) (not shown) and 4-vinyl H_βs (Figure 4F) that is diagnostic for Ser39(C4). The position of assigned residues and the key dipolar contacts are illustrated schematically in Figure 1.

The two remaining, upfield-shifted, nonheme methyl groups exhibit T_1s $\approx$ 50 ms and $R_{Fe} \approx 6$ Å that can only arise from the two methyls of Val100(FG4). In accord with this interpretation, a weak cross-peak is observed by one to the 5-CH_3, as well as to Phe42(C7) (Figure 5C), which leads to the stereospecific assignment to the two methyls. Weak NOESY cross-peaks between these two methyls (Figure 5C), as well as to a strongly relaxed single proton and strong NOESY cross-peaks to a less strongly relaxed but upfield shifted protons (Figures 4C, 5C) are consistent with the expectation[47] for the $C_\beta H$ and $C_\alpha H$ of Val100(FG4). The expected His95(F8) $C_{\beta 1}H$ to Val100(FG4) $C_\beta H$ NOE is also observed (Figure 4C).

The assignment of other aliphatic protons is facilitated by first considering aromatic rings. The TOCSY spectra for the aromatic spectral window display numerous connectivities for aromatic rings (not shown; see Supporting Information). A TOCSY-detected, two-spin system (Figure 4E) with one strongly relaxed ring proton exhibits an NOESY cross-peak to Val100-(FG4) $C_{\gamma 1}H_3$ (Figure 4C), as expected[47,70] solely for $C_\delta H$ of Phe105(G5). The C_δHs also exhibits NOESY cross-peaks to a low-field shifted AMX fragment (not shown) whose $C_\alpha H$ also exhibits an NOESY cross-peak to the 3-CH_3 (Figure 4H), as expected for the backbone of Phe105(G5). The $T_1 \approx 40$ ms for the broad Phe105(G5) C_ϵHs peak (Figure 2A, D) is consistent with the expected distance in the crystal structure; the $C_\zeta H$ at $R_{Fe} \approx 4$ Å is expected to be extremely broad with $T_1 < 5$ ms. An upfield shifted, three-spin aromatic ring (not shown; see Supporting Information) exhibits NOESY cross-peaks to both 1-CH_3 (Figure 4B) and Arg70(E14) (Figure 4D), as expected solely for Phe74(E18). A low-field shifted, three-spin ring exhibits numerous intense NOESY cross-peaks to a very weakly shifted Phe ring (Figure 4E), with inter-ring contacts that are unique to the Phe28(B9) and Phe122(H15) rings. Both the 1-CH_3

(70) Bolognesi, M.; Coda, A.; Frigerio, F.; Gatti, G.; Ascenzi, P.; Brunori, M. *J. Mol. Biol.* **1990**, *213*, 621−625.

Table 2. ^{1}H NMR Spectral Parameters for Dipolar-Shifted Heme Pocket Residues in *Aplysia Limacina* Deoxy Mb

							case I		case II		T^{-1} plot[k]		T^{-2} plot[m]	
residue	proton	δ_{DSS}(obs)[a]	T_1,[b] ms[calc][c]	R_{Fe},Å[d]	δ_{DSS}(dia)[e]	δ_{dip}(obs)[f]	δ_{dip}(calc)[g]	δ_{DSS}(calc)[h]	δ_{dip}(calc)[j]	δ_{DSS}(calc)[j]	slope	δ_{int}	slope	δ_{int}
Phe28(B9)	C_δHs	7.05		10	6.6	0.4	0.8		0.4		0.5	5.4	0.8	6.2
	C_ϵHs	8.46	∼200	8.5	7.4	1.0	2.6		0.9		1.3	4.2	2.0	6.4
	C_ζH	8.85	∼200	8.5	7.6	1.2	3.3		1.1		1.5	4.2	2.2	6.3
Ser39(C4)	C_αH	4.15		10	5.0	−0.9	−0.1		−0.7		−0.5	5.7	−0.7	4.9
	$C_{\beta1}$H	4.46		8.7	4.5	0.0	0.6		−0.1		−0.2	4.9	−0.2	4.6
	$C_{\beta2}$H	4.50		10	4.5	0.0	0.6		−0.3		0.0	4.5	−0.1	4.5
Phe42(C7)	C_αH	2.71		10	4.5	−1.8	−1.2		−1.7		−1.4	7.1	−2.1	4.9
	$C_{\beta1}$H	−0.24		7.7	3.8	−4.1	−2.7		−3.9		−3.1	9.6	−4.7	4.6
	$C_{\beta2}$H	0.49		7.7	3.6	−3.1	−2.6		−3.2		−2.1	7.3	−3.2	3.9
	C_δHs	6.01		9.4	7.7	−1.7	−1.2		−1.9		0.1	10.4	−2.1	8.2
	C_ϵHs	6.42		11	7.6	−1.2	−0.6		−1.1		−8.2	9.1	−1.3	7.7
	C_ζH	6.53		12	7.5	−1.2	−0.5		−1.3		−4.4	7.9	−0.7	7.3
Phe43(CD1)	C_αH	3.52		8.1	4.7	−1.2	−1.8		−1.3		−7.6	6.6	−1.6	5.2
	C_δHs			7.5	7.2		−2.5	4.8	0.0	7.2				
	C_ϵHs		[30][c]	5.5	5.9		−6.3	−0.4	2.9	8.8				
	C_ζH		[7][c]	4.3	3.6		−8.7	−5.1	6.0	9.6				
Ile67(E11)	C_αH	−6.00	35	5.5	3.8	−9.8	−7.2		−9.5		−7.2	17.4	110	5.8
	C_βH		[120][c]	6.7	1.1		−3.1	0.7	−1.7	−0.6				
	$C_\gamma H_3$	−1.98	45	6.1	1.1	−3.1	−0.1		−2.6		−1.3	2.3	34.	1.5
	$C_{\gamma1}$H	[−5.1]	[3][c]	3.7	−1.9		−12.1	−14.0	−3.2	−5.1				
	$C_{\gamma2}$H	[−15.1]	[12][c]	4.7	−2.8		−14.8	−17.6	−10.8	−13.6				
	$C_\delta H_3$	[0.8]	[20][c]	5.0	−3.6		−4.4	−8.0	4.4	0.8				
Arg70(E14)	C_αH	2.84		9.9	4.4	−1.6	−1.2		−1.8		−1.2	6.6	−1.8	4.7
	$C_{\beta1}$H	−2.36	130	7.9	3.3	−5.7	−3.6		−5.2		−4.3	11.5	−6.6	4.5
	$C_{\beta2}$H	−0.57	∼150	7.0	2.7	−3.3	−2.1		−3.2		−2.5	7.5	−3.8	3.4
	$C_{\gamma1}$H	−0.85	∼150	6.9	2.3	−3.1	−2.1		−2.4		−1.7	4.8	−2.7	1.9
	$C_{\gamma2}$H	−1.20		8.2	2.6	−3.8	−3.5		−3.6		−2.9	8.3	−4.5	3.5
	$C_{\delta1}$H	2.01		9.1	3.2	−1.2	−1.2		−1.4		−1.0	5.2	−1.5	3.6
	$C_{\delta2}$H	2.35		9.9	3.2	−0.9	−1.4		−1.2		−0.8	4.9	−1.1	3.5
Leu71(E15)	CγH	2.46		8.5	2.5	−0.1	0.3		−0.4		−1.0	5.4	−1.5	4.0
	$C_{\delta1}H_3$	0.30		10	0.5	−0.2	0.5		−0.6		−1.0	3.4	2.6	1.8
	$C_{\gamma2}H_3$	−0.33		10	0.3	−0.6	0.1		−0.7		−1.7	5.2	1.5	2.4
Phe74(E18)	C_δHs	6.13		10	7.2	−1.0	−0.4		−0.6		−0.7	8.2	−0.9	7.2
	C_ϵHs	5.84		9.5	6.9	−1.0	1.4		−0.6		−0.6	7.8	−1.0	6.8
	C_ζH	5.96		9.5	6.7	−0.8	−1.4		−0.0		0.2	5.3	0.3	5.6
Phe91(F4)	C_δHs			7.0	6.8		−3.0	3.7	0.6	−7.4				
	C_ϵHs		[30][c]	5.4	6.2		0.1	6.1	−1.2	5.0				
	C_ζH		[10][c]	4.5	6.0		2.7	8.7	3.3	9.3				
Phe98(FG2)	C_δHs		[60][c]	6.0	6.7	−	2.0	8.7	−0.6	8.1				
	C_ϵHs		[90][c]	6.5	7.2	-	6.2	13.3	2.2	9.4				
	C_ζH	[9.3]		7.7	7.7	-	4.8	12.5	1.6	9.3				
Val100(FG4)	C_αH	1.29		8.6	3.7	−2.4	−1.7		−2.0		−1.6	6.6	−2.5	3.9
	C_βH	−2.46	[70][c]	6.2	1.2	−3.6	−5.1		−3.9		−2.5	5.5	−3.9	1.6
	$C_{\gamma1}H_3$	−2.80	55	6.1	0.2	−3.0	−2.3		−3.2		−2.2	4.4	−3.5	0.9
	$C_{\gamma2}H_3$	−6.91	45	5.8	0.6	−7.5	−5.7		−7.9		−5.8	12.0	−9.2	2.7
Gln104(G4)	$C_{\beta1}$H	1.29		8.4	2.3	−1.0	1.5		−0.2		−0.6	3.1	−1.5	2.9
	$C_{\beta2}$H	1.53		8.1	2.7	−1.2	0.3		−0.6		−0.2	2.2	−0.3	1.9
	$C_{\gamma2}$H	0.50		9.8	1.9	−1.4	−0.2		−1.4		−1.6	5.5	−2.4	3.0
Phe106(G5)	C_αH	5.06		9.0	4.3	0.8	2.2		1.1		0.6	3.2	0.9	4.1
	$C_{\beta1}$H	3.61		9.9	3.2	0.4	1.1		0.9		0.7	1.4	1.1	2.5
	$C_{\beta2}$H	3.27		10.	2.9	0.4	0.7		0.8		0.5	1.7	0.8	2.5
	C_δHs	8.01		8.0	6.3	0.7	1.5		1.3		0.8	5.4	1.3	6.7
	C_ϵHs	9.06	40	5.7	7.0	2.1	2.4		2.9		2.3	1.5	3.7	5.2
	C_ζH		[5][c]	4.2	3.9	3.9	8.2	12.1	12.7	16.6				
Val108(G8)	$C_{\gamma1}H_3$	1.61		9.5	0.5	1.1	2.6		0.9		0.3	0.6	0.5	1.1
	$C_{\gamma2}H_3$	3.02		8.0	1.3	1.7	4.4		1.7		1.6	−2.3	2.3	0.6
Peak A		13.8	∼10	∼4.5									0.8	5.9
Peak B		11.0	∼10	∼4.5									0.5	6.0
Peak C		10.29	∼30	∼5.5									0.4	5.9

[a] Chemical shifts in ppm referenced to DSS at 36 °C in ^2H_2O at pH 8.6. [b] Observed T_1, (±20% uncertainty), in ms, as estimated from null point, τ_{null}, in an inversion−recovery experiment. [c] T_1 calculated based on eq 6 and the distance given in the metMb crystal structure (47). [d] Distance to the iron, in Å, in the *Aplysia* metMb crystal structure (47). [e] Chemical shifts, in ppm, referenced to DSS for diamagnetic analogue calculated via eq 6 and metMb crystal structure (47). [f] Observed dipolar shift obtained via eq 5. [g] Dipolar shift calculated on the basis of the case I magnetic axes, $\Delta\chi_{ax} = +2.50 \times 10^{-8}$ m^3/mol, $\alpha = 220°$ and $\beta = 88°$, and the *Aplysia* metMb crystal coordinates (47). [h] Predicted chemical shift, referenced to DSS, obtained via eqs 2, 5, and 6 for the case I magnetic axes. [i] Dipolar shift calculated on the basis of the (case II magnetic axes) $\Delta\chi_{ax} = -2.07 \times 10^{-9}$ m^3/mol, $\alpha = 310°$, $\beta = 76°$ and the *Aplysia* metMb crystal structure (47). [j] Predicted chemical shift referenced to DSS, obtained via eqs 2, 5, and 6 for the case II magnetic axes. [k] The slope, in ppm K, and intercept, δ_{int}, in ppm, at $T \rightarrow \infty$, of a plot of δ_{DSS}(obs) versus T^{-1}. [m] The slope, in ppm K, and intercept, δ_{int}, in ppm, at $T \rightarrow \infty$, of a plot of δ_{DSS}(obs) versus T^{-2}.

and the assigned Phe28(B9) ring exhibit (Figure 4D) weak NOESY cross-peaks to another three-spin ring that the crystal structure identifies[47] as Phe134. A two-spin aliphatic system with low-field dipolar shift and intercepts for methyls, has one methyl with NOESY contact to Phe28(B19) (Figure 4E) and another to 3-CH_3 (Figure 4H) which identify $C_{\gamma1}H_3$ and $C_{\gamma2}H_3$ of Val108(G8).

Two partially resolved resonances, a strongly relaxed methyl ($T_1 \approx 40$ ms, $R_{Fe} \approx 5.5$ Å) and a strongly relaxed single proton ($T_1 \approx 30$ ms, $R_{Fe} \approx 5.5$ Å) (Figure 2A, B) fail to exhibit any

TOCSY cross-peaks. The relaxation of the methyl and its NOE to the ring of Phe28(B9) (Figure 4C), however, are diagnostic for the $C_\gamma H_3$ of Ile67(E11). A strong NOESY cross-peak between Ile67(E11) $C_\gamma H_3$ and an aromatic ring identifies the Phe68(E12) ring (Figure 4C); a weak NOESY cross-peak between this ring and Leu71(E15) $C_\delta H_3$ confirms the assignment (not shown). TOCSY detects two four-spin aromatic rings that must arise from the only two Trp, Trp14(A12) and Trp130-(H_{22}). A weak NOESY cross-peak of one Trp to the ring of Phe68(E12) (not shown) and the other to Leu71(E15) (Figure 4D) identify Tyr14 and Trp130, respectively. The 5-CH_3 exhibits an intense NOESY cross-peak to a relatively strongly upfield-shifted proton (Figure 4C) with intercept of an $C_\alpha H$ that must arise from the Phe43(CD1) $C_\alpha H$, and NOESY cross-peaks by a pair of protons to both the 3-CH_3 and 4-vinyl locate the likely $C_\beta HC_\gamma H_2$ fragment of Gln104(G4) (not shown).

Plots of the chemical shift for heme pocket residue protons versus absolute T^{-1} and T^{-2} yield intercepts at $T \rightarrow \infty$, $\delta_{int}(T^{-1})$, and $\delta_{int}(T^{-2})$, as listed in Table 2. The chemical shifts for the assigned residues in an isostructural, diamagnetic analogue are calculated via eqs 5 and 6, on the basis of the crystal structure,[47] and the δ_{DSS}(dia) values are included in Tables 1 and 2. A strong correlation is observed between the expected diamagnetic position for all amino acid residue signals and the intercepts for the T^{-2} (not shown; see Supporting Information) but not the T^{-1} (not shown) correlation. Moreover, a plot of δ_{dip}(obs) versus slope in a shift versus T^{-2} plot is essentially linear (not shown, see Supporting Information) which argues[10,40] for the presence of a single, well-defined molecular structure for the active site and its immediate environment.

Magnetic Axes. The δ_{dip}(obs) for 28 definitively assigned protons with significant dipolar shifts, together with the crystal coordinates of *Aplysia* metMb,[47,70] allowed the determination of both the anisotropy and orientation of the χ tensor. Based on previous work with both mammalian deoxy Mb[40] and ferrocytochromes *c*′,[23,42] where the rhombic anisotropy was found to be much smaller than the axial term, our initial determination was restricted to an axial system, where a search for the degree of tilt, β, and direction of tilt, α, was carried out for the complete range of both angles and $\Delta\chi_{ax}$. A plot of the residual error function, F/n (eq 4), versus $\Delta\chi_{ax}$ in Figure 6 reveals the expected (in fact, required)[71] double minimum, one with a positive $\Delta\chi_{ax}$, case I ($\Delta\chi_{ax} = +2.50 \pm 0.08 \times 10^{-8}$ m^3/mol, $\alpha = 220 \pm 10°$, $\beta = 88 \pm 2°$), one with a negative $\Delta\chi_{ax}$, case II ($\Delta\chi_{ax} = -2.07 \pm 0.08 \times 10^{-8}$ m^3/mol, $\alpha = 310 \pm 10°$, $\beta = 76 \pm 2°$), with the tilt directions for cases I and II differing[71] by ~90°. However, the residual error function for case II is considerably smaller than that for case I (see Figure 6). A plot of δ_{dip}(obs) versus δ_{dip}(calc) for cases I and II are illustrated in Figure 7. It is clear in Figure 7 that case II, with the lower residual F/n, exhibits a remarkably good correlation between observed and predicted δ_{dip}, while the data for case I leads to a correlation where the majority of the data points deviate systematically from the ideal slope of 1, and where the deviation increases in the same direction for large upfield or downfield shifts. In consideration that we have to use the crystal coordinates of *Aplysia* metMb[47] because those of deoxy Mb are not available, extension of this study to quantitate the expected very small $\Delta\chi_{rh}$ for case II was not considered productive and hence abandoned for the present.

The magnetic axes, however, must meet two further conditions to be considered realistic and robust; they must account for strongly relaxed and unassigned resolved signals A, B, C in Figure 2 (aromatic protons), and they cannot predict resolved

(71) The expected double minimum, with opposite sign anisotropies and with a 90° rotation of the major axis, results from the change of sign for both $\Delta\chi$ and the geometric factor, $(3\cos^2\theta - 1)$, for the majority of residues.

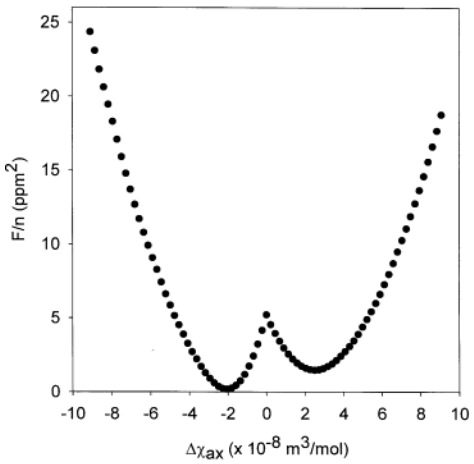

Figure 6. Plot of the residual error function, F/n, (eq 6), upon optimizing the angles β (degree of tilt of major magnetic axis) and α (direction of tilt of major magnetic axis) for all possible positive and negative values of $\Delta\chi_{ax}$. The expected double minima are observed, where the two minima necessarily involve a change in the sign of $\Delta\chi_{ax}$ and an ~90° rotation of the direction of the tilt (such that most of the geometric factors in eq 1 change sign). The two minima are case I, $\Delta\chi_{ax} = 2.50 \times 10^{-8}$ m^3/mol, $\alpha = 220°$, $\beta = 88°$, and case II, $\Delta\chi = -2.07 \times 10^{-8}$ m^3/mol, $\alpha = 310°$, $\beta = 76°$, with the residual error function significantly lower for case II ($F/n = 0.15$) than case I ($F/n = 1.43$).

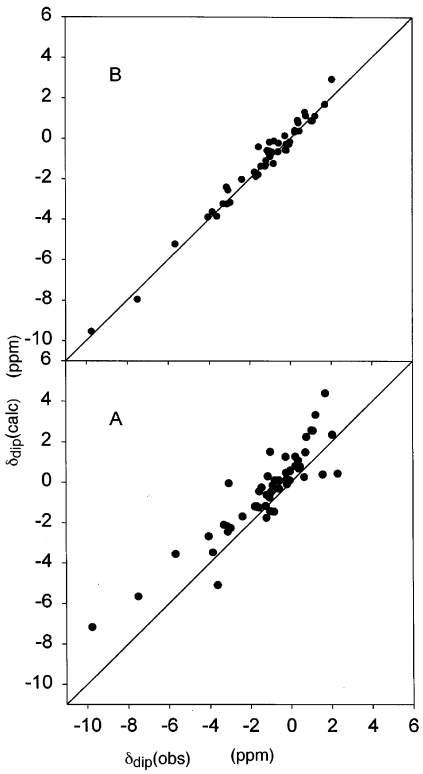

Figure 7. Plot of δ_{dip}(obs), obtained via eqs 4 and 5, versus δ_{dip}(calc) obtained via eq 1, using the magnetic anisotropies and orientation for case I (A) and case II (B), as defined in text and Figure 8. The straight line with unit slope represents an ideal fit. Note the excellent correlation in panel B but the systematic deviations to the upper left in panel A.

signals with weak to moderate relaxation that are not observed. The δ_{dip}(calc) and δ_{DSS}(dia) and eq 6 allow the estimation of the position, δ_{DSS}(calc), and T_1s (via eq 3) for these residues and all unassigned residues which lead to such signals and the relevant data are included in Table 2. For the heme, both cases I (see Supporting Information) and II (Table 1) agree in predicting large upfield δ_{dip}(calc) for β- and δ- and large low-field δ_{dip}(calc) for α- and γ-meso-H. The δ-meso-H is found upfield, but a low-field bias by as little as ~5 ppm would make the β-meso-H undetectable (note: case II predicts ~4 ppm further upfield δ- than β-meso-H shift). The low-field α- and γ-meso-H would resonate under the multiple, less strongly relaxed, low-field peaks and would most likely be undetectable. Hence, the meso-H data only slightly favor case II.

The rings of four strongly relaxed Phes 43(CD1), 91(F4), 98(FG2), and 105(G5) are predicted to exhibit strong to moderate low-field δ_{dip} for case II and provide several candidates for both peaks A and B. While none of these residues predict the T_1 to peak C, it would require a relatively small (0.5 to 1.0 Å) change in R_{Fe} from the metMb crystal structure to account for the observed T_1. It is noted, moreover, that two rings, Phe43-(CD1) and 98(FG2), lie across the nodes in the dipolar field (Table 2), such that their δ_{dip} are probably not accurately predicted. Reduction of metMb to deoxy Mb is expected to lead to a more out-of-plane position of the Fe and, hence, to an increase in R_{Fe} to distal residues. In contrast, case I predicts upfield δ_{dip}(calc) for all but the Phe105(G5) of the same four relaxed rings and, hence, could account, at the most, for one of the three peaks A−C. Hence, the peaks A−C are consistent with case II but not case I.

The CH_2CH_3 fragment of Ile67(E11) is predicted to exhibit large and comparable upfield δ_{dip} for both cases I and II. However, the extreme relaxation predicted for two of the three protons, and the variability of the orientation of the side chain in different crystal structures,[47] indicates strongly relaxed signals that could well be lost under the multiple, less strongly relaxed, upfield peaks. Hence Ile67(E11) does not differentiate between cases I and II. Last, case I predicts strongly upfield shifted and resolved, but only weakly to moderately relaxed, methyl signals for both Leu29(B10) and Val67(E7), and no such signals are observed. In contrast, case II predicts small to moderate low-field shifts which place these signals well within the diamagnetic envelope, as must be the case. Hence, the analysis of predicted shift for unassigned residues signal overwhelmingly favors case II over case I. This analysis leads us to conclude that the presently described orientation and anisotropy of χ as described by case II is both realistic and robust.

Evaluation of Heme Contact Shifts. The qualitative determination of the anisotropy and orientation of χ for case II allows the estimate of δ_{dip} for the heme at 36 °C and, together with the δ_{hf} obtained via eq 8, yields δ_{con}(calc) for each methyl and meso-H, as listed in Table 1. For completeness, we include the δ_{dip}, δ_{con} obtained for case I in the Supporting Information. The δ_{DSS}(obs) for the heme methyls and C_αHs over the 25−45 °C temperature range, together with the estimation δ_{dip}(calc) at each temperature (determined by the T^{-2} scaled δ_{dip}(calc) deduced at 36 °C via case II), result in the heme methyl and C_αHs δ_{con} for each temperature. The resulting heme δ_{con}(calc) values are plotted versus T^{-1} (Curie plot) in Figure 8. It is clear in Figure 8 that the three upfield methyls exhibit considerably steeper than T^{-1} (Curie) behavior predicting sign changes of δ_{con} in the 50−120 °C range, while the low-field 3-CH_3 and propionate C_αH peaks exhibit much closer to T^{-1} (Curie) behavior.

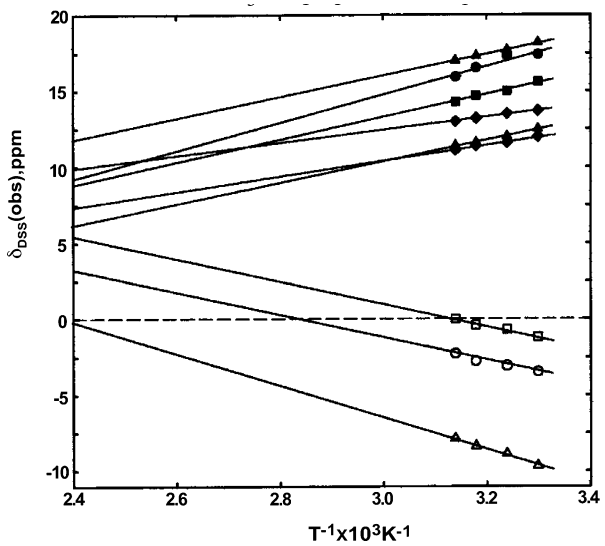

Figure 8. Plot of heme methyl δ_{con} versus T^{-1} (Curie plot), obtained via eqs 4 − 5 based on δ_{DSS}(obs) over the temperature range 30−45 °C and δ_{dip}(calc) at 36 °C, where the magnetic axes were determined, and with δ_{dip}(calc) scaled by T^{-2}, as demanded by the $\delta_{int}(T^{-2}) \approx \delta_{DSS}$(dia). The data illustrated include 1-CH_3 (△), 3-CH_3 (▲), 5-CH_3 (□), 8-CH_3 (○), 2-H_α (●), 6-H_αs (■), and 7-H_αs (◆) contact shifts.

Discussion

Magnetic Properties. The quantitative fit of the observed and predicted dipolar shifts, as illustrated in Figure 7B, the consistency of the observed resolved resonance with prediction of dipolar shifts for unassigned residues in the heme cavity, and the good correlation between the δ_{DSS}(dia) calculation via eq 6 and the intercepts at $T \rightarrow \infty$ in a shift versus T^{-2} plot, $\delta_{int}(T^{-2})$ (Supporting Information) lead to four important conclusions. First, χ exhibits essentially *axial symmetry*; second, the *axial anisotropy is negative*, $\Delta\chi_{ax} = -2.07 \times 10^{-8}$ m^3/mol; third, the *major magnetic*, (*z*−), *axis is tilted nearly into the heme plane* ($\beta = 76°$) in the approximate direction, $\alpha = 310°$, of the α-meso position (see Figure 1); and last, the *anisotropy arises predominantly from zero-field splitting* that accounts for the T^{-2} dependence of dipolar shifts[40,42] and where the observed $\Delta\chi_{ax}$ translates to $D \approx 20$ cm^{-1}.

It is noted that the tilt direction of χ is within 5° of the axial His imidazole plane orientation.[47] Strong tilting of the major magnetic axes well off the heme normal has been reported for the other extensively studied high-spin ferrous hemoproteins.[23,40,42] No structural bases have been offered for these observations, and the present study does not enlighten us further. It is expected that the results of similarly quantitative ^{1}H NMR studies of other crystallographically characterized deoxy globins from a variety of genetic origins will be necessary before a pattern emerges.

Comparison with Other High-Spin Ferrous Hemoproteins. The present *Aplysia* deoxy Mb ^{1}H NMR study is consistent with those on mammalian deoxy Mb's and ferrocytochrome *c*′ in that they agree that dipolar shifts exhibit strictly T^{-2} dependence that dictates they all arise from zero-field splitting.[40,42] The mammalian deoxy Mb complexes (human, horse, sperm whale)

differ from *Aplysia* Mb in exhibiting magnetic anisotropy[40] whose magnitude is half as large as that observed presently. Moreover, a determination of the magnetic axes for sperm whale deoxy Mb leads to the expected double minimum with different signs for the axial anisotropy and ~90° rotation of the major axis,[71] but the quality of the NMR data were insufficient to clearly distinguish whether the positive and negative signs of $\Delta\chi_{ax}$ are, in fact, correct. This ambiguity in the sign of $\Delta\chi_{ax}$, which has not been resolved to date, can be traced to the availability of fewer assignments[40] with less certainty in the mammalian Mb's than *Aplysia* deoxy Mb. The fewer and less certain assignments for the mammalian deoxy Mbs, in turn, can be traced to the much more severe spectral congestion than in *Aplysia* deoxy Mb's, and this problem is due to the much smaller magnetic anisotropy and, hence, increased spectral congestion in the former complexes. It is noted that the total spectral spread for mammalian Mb's[35,38−40,67,72] (~22 ppm) is only half that for *Aplysia* deoxy Mb (~42 ppm). Since the heme methyl T_1s ≈ 50 ms are comparable for all deoxy globins studied to date[35,38−40] and exhibit strong Curie relaxation,[67] increasing the magnetic field to improve dispersion in mammalian deoxy Mbs leads to poorer, rather than better, resolution for the strongly to moderately shifted protons. It is clear that, in the mammalian deoxy Mb's, progress will be made in defining χ only if the protons which experience small δ_{dip}, but are sufficiently far from the iron so as to experience negligible Curie relaxation, can be assigned by standard sequence-specific approaches using ^{15}N labeled globin chains. Such studies are planned on sperm whale deoxy Mb.

The $\Delta\chi_{ax}$ described for *Aplysia* deoxy Mb is very similar in magnitude, but *opposite* in sign, to the quantitatively characterized magnetic axes/anisotropy reported[23,42] for *R. capsulatus* ferrocytochrome *c*′. The major magnetic axis is also tilted significantly from the heme normal in the cytochrome *c*′ (~30°), but in a direction approximately perpendicular to the axial His imidazole orientation, although the imidazole is oriented similarly with respect to the heme in those two hemoproteins.[47,73] It is not possible at this time to assess the reasons for these differences.

Nature of the Heme Contact Shifts and Spin Delocalization. The determination of robust magnetic anisotropy and orientation for *Aplysia* deoxy Mb allows the calculation of δ_{dip}(calc) for the heme substituent and, via eq 6, the estimation for δ_{con}. The δ_{con} values for case II are listed in Table 1 (similar data for case I are given in Supporting Information), which can be compared with the previously reported factored δ_{con} for the same substituents for sperm whale deoxy Mb[40] and *R. capsulatus* ferrocytochrome *c*′[42] (last two columns). The most striking result is the remarkably similar contact shift pattern for *Aplysia* deoxy Mb and ferrocytochrome *c*′,[42] as well as other[41] ferrocytochromes *c*′, both of which differ, qualitatively and quantitatively, from those in mammalian deoxy Mb's.[40] The similarity in the pattern, together with the similar axial His plane orientations along the general α, γ-meso axis for *Al* deoxy Mb[47] and ferrocytochromes *c*′,[73] shows for the first time that, even though the zero-field splitting and the orientation may differ, similar His orientations lead to very similar contact shift patterns. It had been proposed[19,41] that the heme methyl hyperfine shift pattern characteristic of ferrocytochromes *c*′ and *Aplysia* deoxy Mb with similar axial His orientation is the result of the dipolar shifts due to the magnetic anisotropy. It is clear in Table 1 that the upfield 1, 3, 5-, 8-CH_3 and the downfield 3-CH_3 hyperfine shifts are primarily due to contact, rather than dipolar shifts.

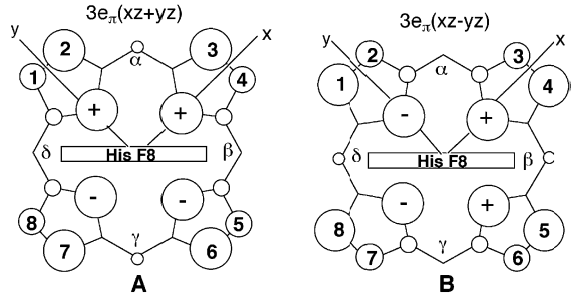

Figure 9. Schematic representation of the distribution of the majority of the spin density (density ∝ size of circle) over the symmetry-adapted porphyrin MOs that can interact with the two dπ orbitals on iron: (A) 3e$_\pi$-($xz + yz$) capable of interacting only with d($xz + yz$) and (B) 3e$_\pi$($xz - yz$) capable of interacting solely with d($xz - yz$).

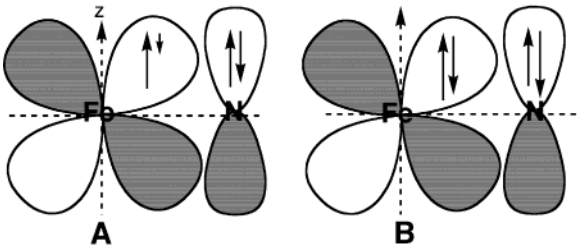

Figure 10. Schematic depiction of the mechanism that leads to positive or negative π spin density in the porphyrin. (A) The singly occupied d$_\pi$ possesses one parallel (positive) spin, and the porphyrin 3e$_\pi$ MO possess paired spins. Donation of a fraction antiparallel (negative) spin to the singly occupied d$_\pi$ leaves a fraction parallel (positive spin) in 3e$_\pi$ MO. (B) Both dπ and 3e$_\pi$ are doubly occupied. Spin−spin correlation with the four parallel spins on Fe results in favoring parallel (positive) spin in d$_\pi$, which results in net antiparallel (negative spin) in 3e$_\pi$. Note the unequal lengths of the positive and negative spin arrows for both the iron and porphyrin π MO in B.

The heme contact shift pattern is characterized by relatively small, both upfield and downfield, δ_{con} that is approximately 2-fold symmetric with respect to the axial His plane (along the β-,δ-meso vector), all of which argues for the predominance of π-spin delocalization over the heme. Moreover, the relative small δ_{con} for the δ-meso-H dictates that the filled 3e$_\pi$ orbitals, rather than vacant 4e$_\pi$ porphyrin molecular orbitals, MOs, interact with the π-bonding d orbitals.[5,74,75] For the coordinate system in Figure 1, the two 3e$_\pi$ MOs, 3e$_\pi$(xz+yz) and 3e$_\pi$(xz−yz), which interact with the d$_\pi$ orbitals ($xz + yz$) and ($xz - yz$), respectively, are shown in Figure 9A and B. The pattern of contact shifts (see below) dictates that the orbital ground state in axial symmetry arises from $[(xz + yz)(xz - yz)]^3(x^2 - y^2)$-$(z^2)(xy)$; in lower symmetry, the two d$_\pi$ levels are split. The positive π spin density (low-field δ_{con} for C_αH's) at positions 2−, 3−, 6−, and 7− (Table 1) thus dictates that the ground state has a singly occupied ($xz + yz$) that results in direct (*positive*) spin delocalization by transfer of partial spin to 3e$_\pi$-(xz+yz), as illustrated in Figure 10A. The upfield C_αH δ_{con} for

(72) Wüthrich, K. *NMR of Proteins and Nucleic Acids*; Wiley & Sons: New York, 1986.
(73) Tahirov, T. H.; Misaki, S.; Meyer, T. E.; Cusanovich, M. A. *J. Mol. Biol.* **1996**, *259*, 467−479.
(74) La Mar, G. N.; Walker, F. A. In *The Porphyrins*; Dolphin, D., Ed.; Academic Press: New York, 1978; Vol. IV, pp 61−157.
(75) Walker, F. A. In *The Porphyrin Handbook*; Kadish, K. M., Smith, K. M., Guilard, R., Eds.; Academic Press: Boston, 1999; Vol. 5, pp 81−183.

positions 1−, 4−, 5−, and 8− (Table 1) dictate that *negative* π spin density appears in $3e_\pi(xz-yz)$ (Figure 9B). Such negative π spin can be expected on the basis of spin−spin correlation between the four (positive) unpaired iron spins and the paired spins in $(xz - yz)$, which results in net *negative* π spin density in the $3e_\pi(xz-yz)$, as depicted schematically in Figure 10B. Thus the orbital ground state places moderate positive π spin density into $3e_\pi(xz+yz)$ and small negative π spin density into $3e_\pi(xz-yz)$ and accounts for the observed δ_{con} pattern over the heme.

The first excited orbital state, $(xz + yz)^2(xz - yz)(x^2 - y^2)(z^2)(xy)$, however, reverses the effect by placing positive π spin into $3e_\pi(xz-yz)$ and negative π spin into $3e_\pi(xz+yz)$. The thermal population of this excited orbital state would lead to sizable low-field δ_{con} for $C_\alpha H$'s at positions 1−, 4−, 5−, and 8− and accounts for the considerably steeper than T^{-1} behavior for 1-CH_3, 5-CH_3, and 8-CH_3 (Figure 8), predicting sign changes in the temperature range −50° to 20 °C. Such temperature data for δ_{DSS}(obs) has not been reported for the other high-spin ferrohemoproteins studied in detail, so the generability of this effect cannot be gauged at this time. Similar anomalous non-Curie temperature behavior in the case of low-spin iron(III) has been shown to be characteristic of thermal populations in two orbital states.[4,5,11−14] It is predicted that the same upfield shifted heme methyls in ferrocytochromes *c*′ will exhibit the anomalous temperature behavior observed here and that a similar orbital ground state is occupied. The mammalian deoxy Mb's fail to exhibit any heme methyl or propionate $C_\alpha H$ with upfield δ_{con}, which would imply a smaller orbital splitting, and hence a greater population of the excited orbital state. The limited reported temperature data are consistent in that the $C_\alpha H$'s at pyrroles B and D exhibit larger deviations from Curie behavior than the $C_\alpha H$'s on pyrroles A and C.[40] A difference in the orbital splitting between mammalian and *Aplysia* deoxy Mb is supported by the difference in the magnitude of the magnetic anisotropies and, hence, *D* values.

The presently proposed correlation mechanism which gives rise to negative ρ_π spin density in the $3e_\pi$ MO that interacts with the doubly occupied d_π should manifest itself similarly in low-spin iron(III) hemoproteins. However, upfield δ_{con} for heme $C_\alpha Hs$ have not been reported to date. This strongly enhanced effect of the spin correlation that results in this *significant* negative π spin density on the heme in $S = 2$ iron(II), but none or little in $S = {}^1/_2$ iron(III) hemes, is completely consistent with the fact that the paired spins in the filled d_π are much more effectively correlated by the four unpaired spins in the former, than the single unpaired spin in the latter oxidation/spin state. The potential presence of this correlation effect in $S = {}^1/_2$ ferrihemoproteins, however small, would interfere with the quantitative interpretation of hyperfine shift patterns in terms of ligand orientation(s)[14,15,76,77] and of the temperature dependence of the shifts in terms of the orbital spacing.[12,13] Recent detailed theoretical calculations of spin density for low-spin ferriheme models have proposed[78] the presence of both positive and negative π-spin density on the heme.

It is clear that an improved understanding of the NMR spectra of high-spin ferrous hemoproteins requires not only the determination of the anisotropy and orientation of the paramagnetic susceptibility tensor from a variety of proteins with varied active site geometry but also the detailed study of the temperature dependence of both dipolar and contact shifts.

Acknowledgment. The authors are indebted to Drs. M. Brunori and F. Cutruzzolá for providing *Aplysia* Mb. This research was supported by grants from the National Institutes of Health, HL 16087 (G.N.L.) and HL 22252 (K.M.S.). Dedicated to the memory of Eraldo Antonini, eminent biochemist, prematurely deceased twenty years ago, on March 19th, 1983.

Supporting Information Available: Five figures (partially relaxed spectra, low-field and high-field TOCSY spectra, plot of δ_{DSS}(dia) versus intercept at $T = \infty$ for T^{-2} plot, and plot of T^{-2} slope of δ_{DSS}(calc) versus δ_{dip}(obs)) and two tables (factored heme δ_{dip}, δ_{con} for case 1 magnetic axes and chemical shifts for assigned residues with insignificant dipolar shifts) (total 8 pages). This material is available free of charge via the Internet at http://pubs.acs.org.

JA035256U

(76) Bertini, I.; Luchinat, C.; Parigi, G.; Walker, F. A. *J. Biol. Inorg. Chem.* **1999**, *4*, 515−519.
(77) Turner, D. L.; Brennan, L.; Messias, A. C.; Teodoro, M. L.; Xavier, A. V. *Euro. Biophys. J.* **2000**, *29*, 104−112.
(78) Johansson, M. P.; Sundholm, D.; Gerfen, G.; Wilkström, M. *J. Am. Chem. Soc.* **2002**, *124*, 11771−11780.